



HAL
open science

Firing tests of hybrid engine with varying oxidizer nature and operating conditions

Nicolas Gascoin, Alexandre Mangeot, Camille Marin, Philippe Gillard, Dominique Piton, Stéphane Rouvreau, Jacques Prevost

► **To cite this version:**

Nicolas Gascoin, Alexandre Mangeot, Camille Marin, Philippe Gillard, Dominique Piton, et al.. Firing tests of hybrid engine with varying oxidizer nature and operating conditions. Proceedings of the Institution of Mechanical Engineers, Part G: Journal of Aerospace Engineering, 2013, 10.2514/6.2013-4047 . hal-01253266

HAL Id: hal-01253266

<https://hal.science/hal-01253266>

Submitted on 9 Jan 2016

HAL is a multi-disciplinary open access archive for the deposit and dissemination of scientific research documents, whether they are published or not. The documents may come from teaching and research institutions in France or abroad, or from public or private research centers.

L'archive ouverte pluridisciplinaire **HAL**, est destinée au dépôt et à la diffusion de documents scientifiques de niveau recherche, publiés ou non, émanant des établissements d'enseignement et de recherche français ou étrangers, des laboratoires publics ou privés.

Firing tests of hybrid engine with varying oxidizer nature and operating conditions

Nicolas Gascoin^{1a}, Alexandre Mangeot^{a,c}, Camille Marin^b, Philippe Gillard^a, Stéphane Rouvreau^b, Jacques Prevost^b
and Dominique Piton^b

^a*University of Orléans, France*

^b*Roxel France, France*

^c*Centre National d'Etudes Spatiales, France*

Abstract

Hybrid combustors are of increasing interest for space and civilian propulsion. A test facility has been settled to investigate the high density polyethylene combustion (propellant of 0.15 m long). A parametric study has been achieved on the oxidiser nature (gaseous oxygen diluted in nitrogen, from 31.4 vol.% to 69.2 vol.% of O₂), on the oxidiser flow rate (from 28.6 g.s⁻¹ to 53.1 g.s⁻¹), on the combustor pressure (from 11.4 bar to 25 bar) and on the nozzle diameter (from 6.4 mm to 12.9 mm). The regression rate has been estimated by weight loss (mean value of 0.207 mg.s⁻¹) and by thermocouples (0.198 mg.s⁻¹). Its values are compared to existing data through the Marxman law; this enlarges the range of validity of this law. The conduction heat flux in the solid reducer is estimated around 6000 W to 8000 W; which is related to the low regression rate of the solid fuel. The axial thrust has been measured in addition to other parameters (pressures, temperatures, mass flow rates). Solid particles have been gathered at the combustor outlet to conduct additional chemical analyses. These particles were formed at the surface of the reducer and extracted by the oxidizer from the solid surface.

Keywords

Hybrid rocket engine; combustion; high density polyethylene HDPE; regression rate; Marxman law.

¹ Corresponding author : Nicolas Gascoin, University of Orléans, 63 avenue de Lattre de Tassigny, 18020 Bourges Cedex France, Email: nicolas.gascoin@univ-orleans.fr

22 **Introduction**

23 Hybrid rocket engine involves classically a solid fuel (generally Polybutadiene, Polyethylene, or others [1]-[5])
24 and a pressurised oxidiser (such as gas/liquid oxygen, peroxide hydrogen, nitrous oxide [1],[5]). The simple oxidiser
25 injection through a valve, which can be regulated [6], and the gaseous combustible generation thanks to the
26 combustion heat flux [1] make this propulsion mode to be of increasing interest, specifically for space and civilian
27 applications [7]-[10]. The hybrid rocket engines are safe (due to the separate storage of the fuel and of the oxidiser).
28 They may be extinguished and reignited during the flight and the thrust can be varied over the time [7]. Numerous
29 studies do exist, either numerically [11]-[13] or experimentally [14]-[17]. A number of test facilities enable to
30 consider large size engines with thrust over 250 kN [17]. A high number of test benches dedicated to hybrid rocket
31 technology are available at reduced scale (lab conditions) or large scale (demonstrator). Some specific mock-up
32 provide data on "isolated" phenomena (regression rate, pressure effect, combustion instabilities and related pressure
33 oscillations, oxidizer injection, ignition device, addition of compounds in solid reducer, formation of a liquid fuel
34 layer) [18]-[23].

35 Among the available fuels, the high density polyethylene (HDPE) has been studied in several papers [24]-[27].
36 Its regression rate is estimated around 0.4 mm.s^{-1} to 0.8 mm.s^{-1} with nitrous oxide or oxygen; which is quite low
37 compared to other fuels. The major advantage of HDPE is its cost and its ease to be purchased and used. Liquefying
38 fuels and additives are investigated since they present higher regression speed. The regression rate and the liquid
39 surface interface, in case of liquefying fuel, are often measured by ultrasonic methods but thin thermocouples are
40 also of great interest for simplicity of use, post-processing and cost reason [1]. Visualization is also feasible but the
41 modification of the refractive indices, due to unstable liquid layer, heat transfer and mass transfer, makes it difficult.

42 Despite the knowledge which has been developed since over 40 years, the industrial and research communities
43 are still looking for a way to enhance the reducer regression rate in order to increase the engine thrust. Indeed, the
44 major drawback of hybrid engines is due to the fact that the combustion heat release is limited and the resulting
45 combustible formation, on the basis of the solid reducer pyrolysis, is quite low. To cope with the regression
46 limitation, the University of Orléans (France), the Roxel company and the French Space Agency (CNES) have
47 settled a collaboration since 2009 through the CHARME project (French acronym for Hybrid Chamber with
48 Reactive Approach by Modelling and Experiments). A Computational Fluid Dynamics (CFD) code is currently
49 under validation. An experimental test bench at reduced scale (less than one meter long) is also proposed in the

50 framework of the CHARME project in order to validate the CFD code and to test transient configurations by
51 adjusting the oxidiser flow rate.

52 The purpose of this paper is to present the test facility and the associated results which were obtained under quasi
53 steady-state firing configurations. In addition to several measures such as the thrust, the pressure, the flow rates and
54 the temperatures in the system, several thermocouples enable to monitor the regression rate of the solid reducer over
55 the time, axially and longitudinally in the engine. These data present a strong interest to determine the relationship
56 between pyrolysis and combustion. Furthermore, the data are analysed in light of the Marxman law [28] and
57 chemical analyses of the fuel and of the combustion residue are proposed.

58 **Materials and methods**

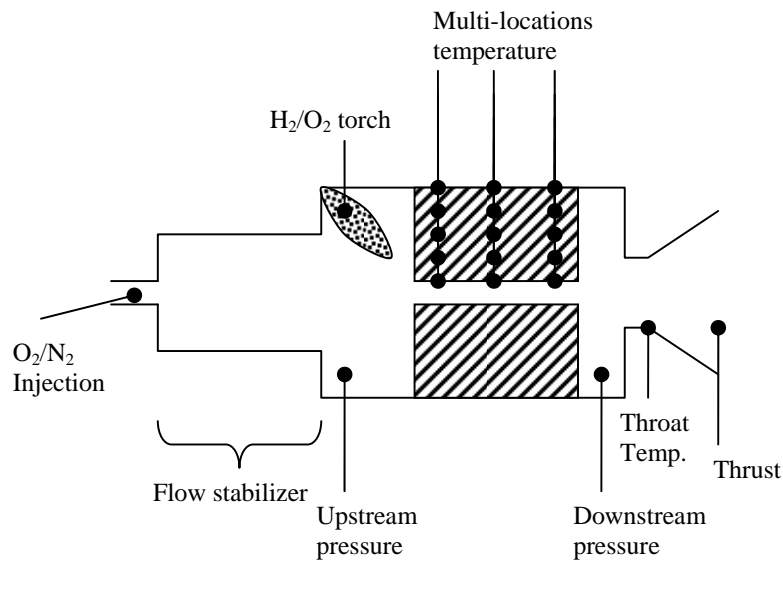
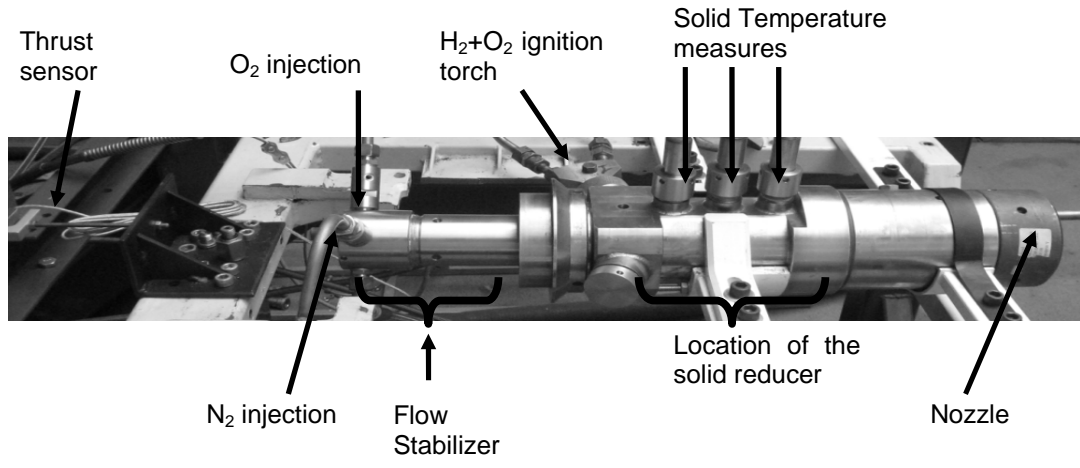
59 *The CHARME test bench*

60 The oxidiser injection, the torch ignition, the solid reducer, the nozzle and the thrust sensors are shown on
61 **Figure 1a**. The corresponding schematic (**Figure 1b**) shows the location of additional measures, such as the
62 temperature and the pressure -upstream and downstream the solid reducer-. It should be noticed that the thrust is
63 mainly given for illustrative purpose since the nozzle appeared not to be adapted to the flow. As a matter of fact, a
64 clear separation of the jet flow is visible during the experiments, which impacts the quantitative use of the thrust
65 measurements.

66 The stainless steel mock-up is internally coated by in-house thermal protection made of carbon-based composite
67 ceramic. The nozzle is made of carbon to withstand the large heat load. The solid reducer is the High Density
68 Polyethylene (solid grain of 0.15 m long with single port, external diameter of 0.09 m and internal one of $4 \cdot 10^{-2}$ m).
69 HDPE is provided by Politek (PE1000). The gaseous oxidiser is a tuneable mixture of O_2 and N_2 by varying their
70 respective feed pressure injected through sonic throat. A flow stabilizer is used to obtain established flow when
71 entering the combustion chamber -for later use in CFD code validation-. After filling up the combustion chamber
72 with the oxidiser and after reaching the expected pressure (which varies depending on the tests, as it is detailed in
73 next section), a H_2+O_2 torch is used during 0.3 s, which is enough to ensure the ignition of the HDPE.

74 All the sensors signals are acquired at a frequency of 62.5 Hz. Some temperature sensors are used on the outer
75 mock-up surface for safety reason in order to limit its heating (damage of the inner thermal protection). At three
76 different longitudinal locations in the solid reducer, the temperature is measured in order to monitor the solid

77 regression and to estimate the regression rate. Five thermocouples (K-type, stainless steel coated, 1 mm of external
 78 diameter) are positioned every 2 mm to 3 mm along the reducer radius for each of these three longitudinal positions
 79 (Table 1). The solid reducer is weighted before and after the test to check the mass balance.



82 **Figure 1. The CHARME Hybrid rocket test bench (a) and the corresponding schematic (b).**

83 **Table 1. Radial positions of the thermocouples in the solid reducer (r=0mm on the central axis).**

	Longitudinal Position from the upstream HDPE border (m)		
	First position : 23 mm	Second position : 73 mm	Third position : 123 mm
Thermocouple 1	21 mm	21 mm	21 mm
Thermocouple 2	24 mm	24 mm	24 mm
Thermocouple 3	27 mm	27 mm	27 mm
Thermocouple 4	30 mm	30 mm	30 mm
Thermocouple 5	33 mm	33 mm	33 mm

84

85 *Test conditions*

86 For all the tests, the oxidiser nature (concentration of O₂ and of N₂) and its flow rate change depending on the
87 test number (Table 2). The oxidiser flow rate ranges from 10 kg.m².s⁻¹ to 60 kg.m².s⁻¹. The operating pressure is
88 linked to the oxidiser injection and to the nozzle diameter, which slightly varies around 7 mm to 8 mm (Table 2).
89 The test duration varies from 80 s to 102 s, ensuring that most of the solid propellant is consumed. Additional
90 information regarding the five tests is summarized in Table 2. At the end of each test, the combustor is filled with
91 nitrogen to extinguish it and cool it down and to solidify the reducer grain. Each solid fuel is then weighted and
92 geometrically measured to determine the mean regression rate and to observe if this regression is homogeneous
93 spatially.

94

Table 2. Test conditions of the successive hot experiments.

Test number	Répartition (vol.%)		Oxidiser flow rate (g.s ⁻¹)	Initial grain diameter (mm)	Mean combustor pressure (bar)	Initial nozzle diameter (mm)	Test duration (s)
	O2 content	N2 content					
5866	53.6	46.4	28.6	39.7	11.4	7.3	98
5869	31.4	68.6	48.6	39.8	11.5	8.7	102
5870	69.2	30.8	47.8	39.7	12.5	8.8	83
5871	47.6	52.4	53.1	39.6	25	6.4	97
5875	52	48	28.9	51	11.5	7.4	80

95

96 **Results and Discussion**

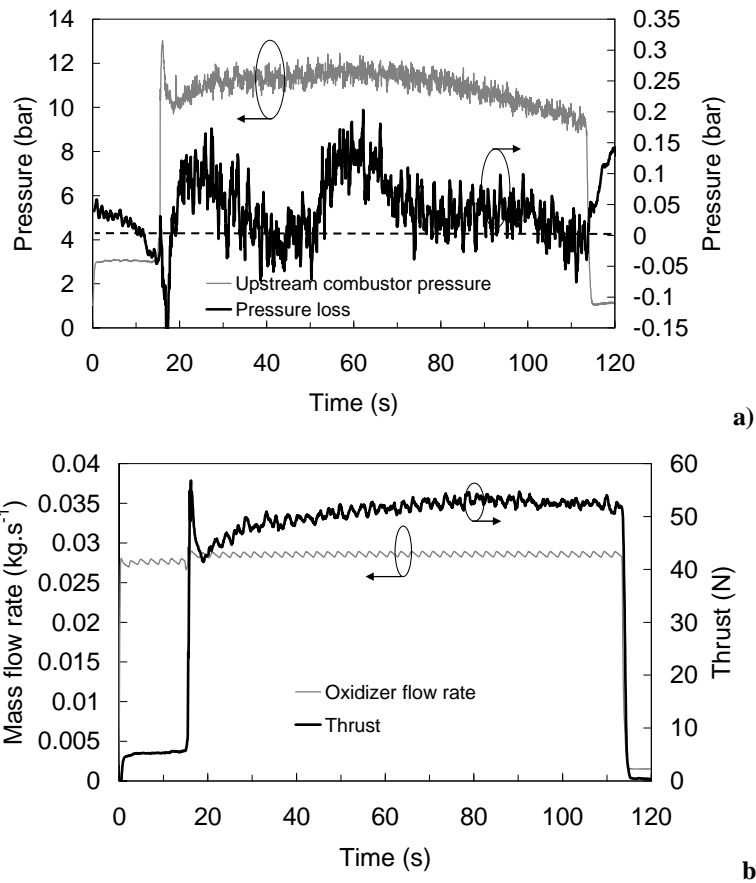
97 *Full post-processing of the test number 5866*

98 **Direct measures of physical parameters.** Thanks to the two pressure transducers (upstream and downstream the
99 reducer), the pressure drop (that is to say the inlet pressure minus the outlet one) is monitored (Figure 2a). Its
100 maximum reaches 0.15 bar for an operating pressure around 11 bar. The ignition effect of the torch is observed
101 around 16 s of experimental time. At this time, the pressure briefly reaches a maximum due to the transient
102 behaviour of the system. Over the entire test length, the pressure remains quite constant up to 75 s and then
103 decreases of about 20 % from 75 s to the end of the test (due to the erosion of the nozzle throat). The pressure drop

104 variations are difficult to understand (Figure 2a). Because of the regression of the solid fuel, the inner port diameter
105 increases. Thus, the pressure drop should decrease (when considering constant oxidizer mass flow rate). This is what
106 is observed from 20 s to 45 s and from 60 s to 110 s roughly. Nevertheless, the pressure drop increases from 45 s to
107 60 s (black curve on Figure 2a). Since the solid regression surface increases during the test due to the axisymmetric
108 geometry, the quantity of pyrolysed fuel increases. This may compensate the pressure drop. This result is interesting
109 because this could show that the pyrolysed fuel flow rate varies during the engine functioning, as it will be seen later
110 in this section. At some time, the combustible flow rate may increase enough during the test to compensate the
111 pressure drop and at other time it may not be sufficient to compensate this pressure decrease due to geometrical
112 changes of the diameter.

113 In addition, the knowledge of the mean fuel flow rate during the test enable to compute the mean equivalence
114 ratio, which is about 1.07 (fuel excess compared to stoichiometric value). The fuel quantity produced during the test
115 is about 10 wt.% to 15 wt.% the one of the oxidiser, that is to say the mixture ratio is around 6 to 10. This varies
116 during the test according to the fuel quantity produced as a function of time -since the oxidiser flow rate remains
117 quite constant (**Figure 2b**)-. The small time-fluctuations, which are observed on the oxidiser flow rate, are due to the
118 inlet pressure regulation system. These oscillations (about 1.2 % of magnitude with a frequency of 0.4 Hz) may be
119 visible on the thrust and the pressure signals in the combustor (frequency of 0.4 Hz and 1 Hz with 5 % and 3.5 % of
120 magnitude respectively). Considering the mean trend, for stabilised flow rate and pressure, the thrust variation is
121 limited (from 44 N to 53 N over the entire test duration from 25 s to 112 s). Moreover, the nozzle throat erosion does
122 not decrease the thrust (**Figure 2b**). Since the nozzle was initially not specifically designed for the test, an
123 explanation is that the throat ablation drives towards a natural adaptation of the nozzle to the flow and pressures. In
124 addition, the nozzle ablation rate remains quite low (about $27 \mu\text{m}\cdot\text{s}^{-1}$, determined by a throat diameter decrease of
125 1 mm over a time of 30 s from 75 s to 112 s). The nozzle throat starts to be consumed around 75 s by the hot gases
126 (nozzle throat diameter varies from 7.3 mm to 8.3 mm during the experiment). This value is estimated on the basis
127 of the pressure decreases in the combustor (seen on **Figure 2a**). For comparison purpose, the nozzle ablation appears
128 after only few seconds for solid fuel engines. This difference between hybrid and solid rockets could be explained
129 by a lower hot gas mass flow rate in the present hybrid engine and by a lower gas temperature compared to real solid
130 propellant systems.

131 It can be mentioned that the temperature of the nozzle throat is measured by a thermocouple inserted 2 mm from
 132 the surface. Nevertheless, the post-processing of this temperature did not furnish a reliable combustion temperature
 133 (about 1200 °C, much lower than the theoretical one of 2680 °C) because of the bad thermal contact with the solid
 134 material.



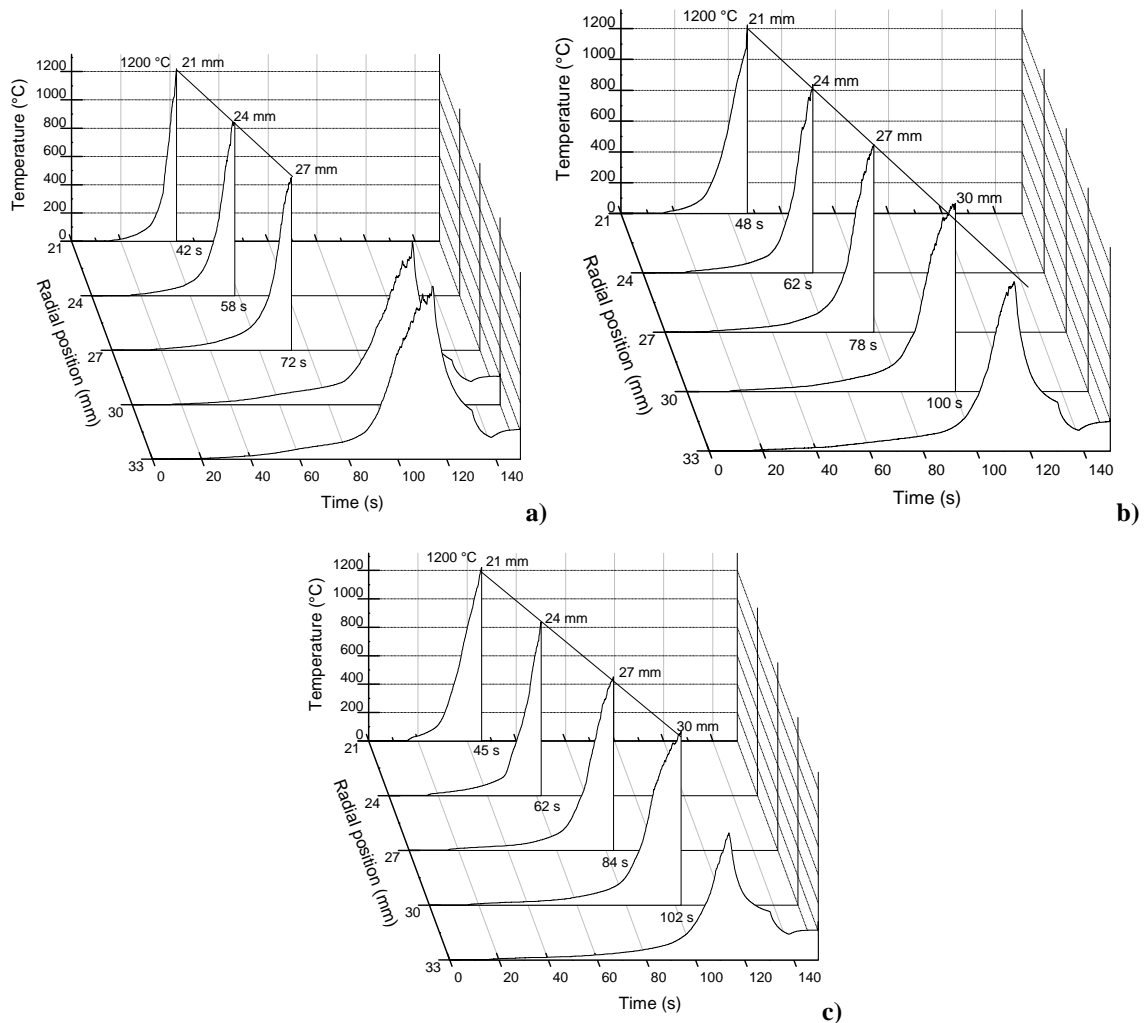
135

136

137 **Figure 2. Pressure and pressure drop (between the inlet and the outlet pressure) histories in the hybrid**
 138 **combustor (a) and thrust with oxidizer flow histories (b) for test case number 5866.**

139 *Thermal investigations of the solid grain.* The temperature measured by each of the fifteen thermocouples along the
 140 three longitudinal positions clearly show that most of the solid reducer has been consumed because almost all the
 141 thermocouples reach 1200 °C (Figure 3). At this temperature, it can be assumed that the thermocouple encounters
 142 the flame because the signal is lost (they get broken). The maximum peaks can be linked by a line for which the
 143 coordinates are marked on each graph. This enables to compute the regression rate. It can be seen that both
 144 thermocouples 4 and 5 (radial position 30 mm and 33 mm) of the first longitudinal position (Figure 3a) reach 1200

145 °C around 120 s. This behaviour does not match with the line linking the three first peak summits. This is probably
 146 caused by a bad insertion in the solid reducer (the position being then erroneous). The last thermocouples (radial
 147 position of 33 mm) of the longitudinal positions 73 mm and 123 mm do not reach 1200 °C because of the end of the
 148 test (Figure 3b and Figure 3c).



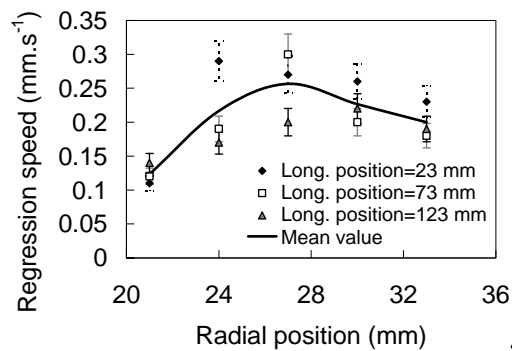
149

150

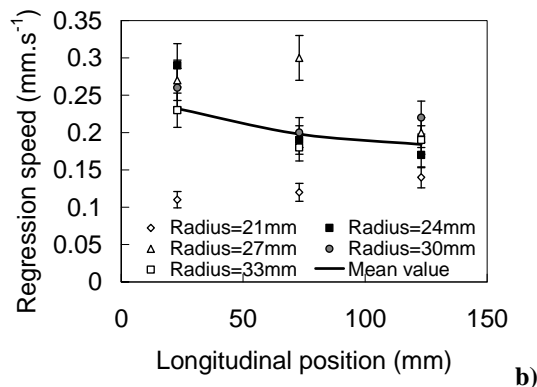
151 **Figure 3. Time histories of the three sets of thermocouples during the test number 5866 from (a) for the**
 152 **upstream position to (c) for the downstream one.**

153 Thanks to these thermal raw data and considering the time to reach the temperature of 1200°C, the regression
 154 rate of the HDPE has been estimated for each thermocouple, knowing their respective positions (**Figure 4**). The
 155 same regression rate estimation has been achieved with 400°C, 600°C, 800°C and 1200°C criteria without
 156 significant changes. The mean regression value of all the data is 0.2 mm.s⁻¹ with variations from 0.11 mm.s⁻¹ to

157 0.30 mm.s^{-1} . Considering the radial position (**Figure 4a**), the regression seems to show a maximum around 28 mm.
 158 The position of this maximum depends in fact of the longitudinal position (24 mm for the first position at 23 mm,
 159 28 mm at 73 mm and 31 mm for the last one at 123 mm). The magnitude of this maximum decreases from the
 160 upstream part of the combustor to the downstream one. Since the error bars correspond to a relative change of 10 %,
 161 this trend is significant. The reason of such a maximum could be linked to the time required for the heat transfer to
 162 be established and to the time variations of the equivalence ratio (the quantity of combustible changes during the test
 163 due to the variation of the regression surface). Accordingly, when plotting the regression rate as a function of the
 164 longitudinal position (**Figure 4b**), the regression decreases along the combustor and this may be attributed again to
 165 the equivalence ratio since the oxidiser concentration decreases along the combustor due to the combustion. The
 166 data for the radius of 21 mm are not similar to the others (**Figure 4b**). This first thermocouple presents a low
 167 regression speed (mean value of 0.12 mm.s^{-1}) compared to others (mean value over 0.20 mm.s^{-1}). This is attributed
 168 to the time required by the bench to get ignited and to reach a steady-state. Thus, this is a way to estimate the
 169 stabilisation time of the system (about 25 s) since the ignition occurs around 18 s (**Figure 2b**) and this thermocouple
 170 is consumed after a time around 42 s (**Figure 3a**), 45 s (**Figure 3b**) and 48 s (**Figure 3c**).



171

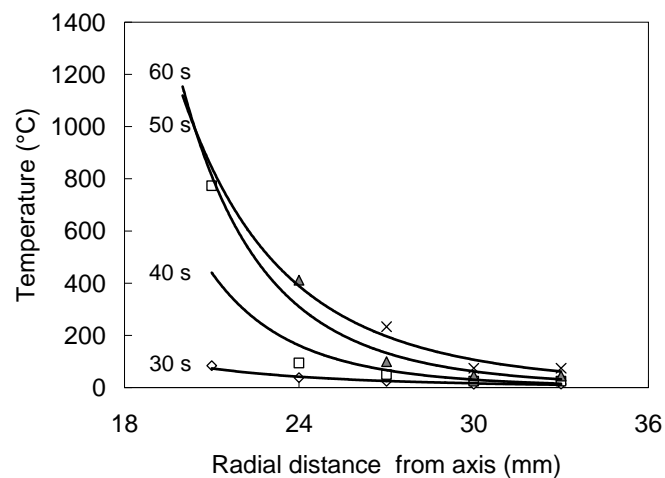


172

173 **Figure 4. Regression speed given as a function of radial (a) and longitudinal coordinates (b) with data from**
174 **test number 5866.**

175 Due to the bad radial position of thermocouples 4 and 5 (radial position 30 mm and 33 mm with uncertainty of
176 1 mm) for the first longitudinal position at 23 mm, the uncertainty on the regression rate determination reaches 18.2
177 % while it is respectively 9.33% and 8.99% for the second and third position.

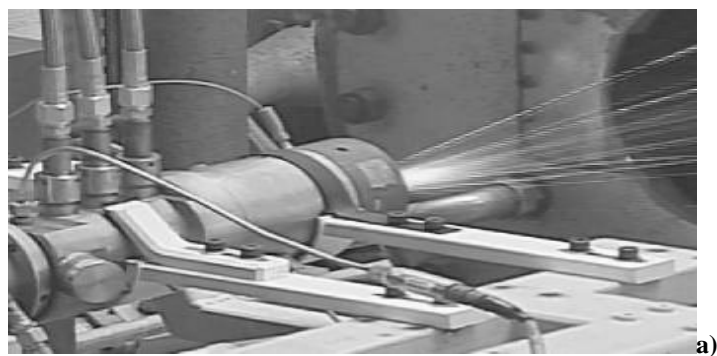
178 The thermocouples also enable to observe the thickness of the thermal boundary layer in the solid fuel (**Figure**
179 **5**); that is to say the relationship between the position and the temperature in the solid fuel. This layer is located in
180 the first three millimetres, that is to say close to the solid-gas interface. In addition, by computing the thermal
181 gradient on the basis of these temperature measures, this observation is confirmed and a maximum value of 230
182 $K.m^{-1}$ is obtained. There was a will to determine if a liquid layer appears during the degradation of the HDPE but
183 the thermocouples signals and their derivation can not allow to answer this point. The liquid film should present a
184 thickness (few micrometres) much lower than the distance between two thermocouples (2 mm to 3 mm) and even
185 lower than the size of the thermocouple itself (1 mm).



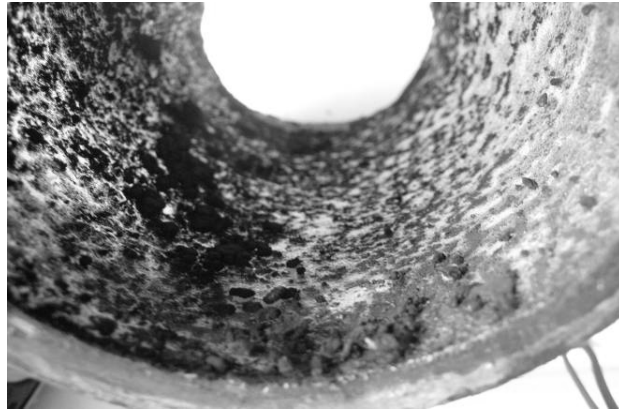
186 **Figure 5. Thermal boundary layer profile at different time step for the test number 5866.**

188 *Chemical investigations of the solid grain.* During the firing tests, ejection of incandescent solid particles is clearly
189 visible (Figure 6a). This tends to demonstrate that the combustion of the solid fuel is not complete. After the test, the
190 observations of the solid grain show the presence of solid black particles on the surface of the white HDPE fuel
191 (Figure 6b). To investigate this point, a collector filled with water has been installed downstream the combustor. The
192 gathered black particles have been studied by complementary tools (Scanning Electron Microscope –SEM– with

193 Electron Dispersive Scanning –EDS- and Fourier Transform Infrared Spectrometer –FTIR-). The images show
194 aggregates (Figure 7a) with different structures: some with small spherical particles (of the order of few nanometres)
195 (Figure 7b) and some large ones (about 4 μm) (Figure 7c). Their analysis by EDS, whatever the size of the spherical
196 particles, presents a high carbon content (over 95 atom.%) with a small complementary oxygen content. In addition,
197 the FTIR analysis by Diffuse Reflection reinforces the chemical analysis by showing the molecules bonds (Figure
198 8a). Hydrogen, carbon and oxygen contents are found. To understand how these oxygenated hydrocarbon particles
199 were formed, a thermal analysis has been achieved with ThermoGravimetric Analysis (Figure 8b). A thermal slope
200 ($20 \text{ K}\cdot\text{min}^{-1}$) up to 1000 K was carried out and the mass loss was monitored under inert (Ar) and oxidative (Air)
201 atmosphere. The pyrolysis under Ar atmosphere shows a mass loss of about 1 wt.% while the same pyrolysis under
202 Air atmosphere presents a mass loss of 80 wt.% (Figure 8b). This tends to demonstrate that the solid particles are
203 formed at high temperature during the pyrolysis process and are not combustion residue or soot particles because
204 they would not react so much in oxidative atmosphere. This result is important because this shows that a part of the
205 solid reducer is transformed in solid particles which are ejected from the combustor without being burned. This is
206 one of the reasons that explain the low regression rate of the HDPE because this unburned part of fuel does not
207 contribute to the combustion and to the generation of the heat flux for the pyrolysis.



208



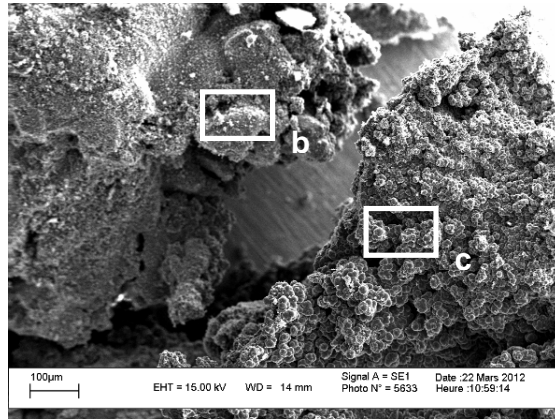
b)

209

210

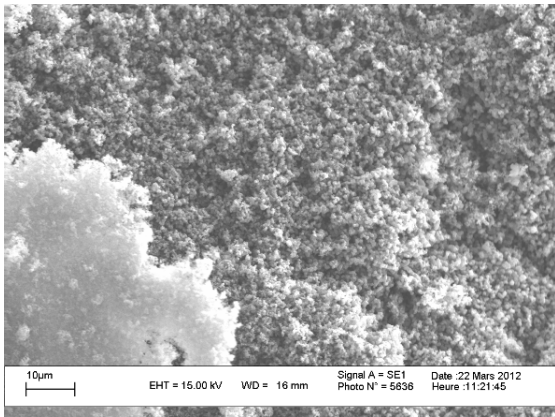
211

Figure 6. Picture of a firing test with incandescent solid particles ejection (a) extracted from the solid reducer surface (b).

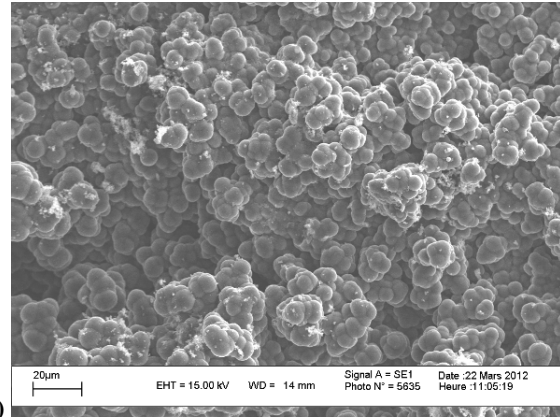


a)

212



b)



c)

213

214

Figure 7. SEM images of the collected solid particles (a-c).

215

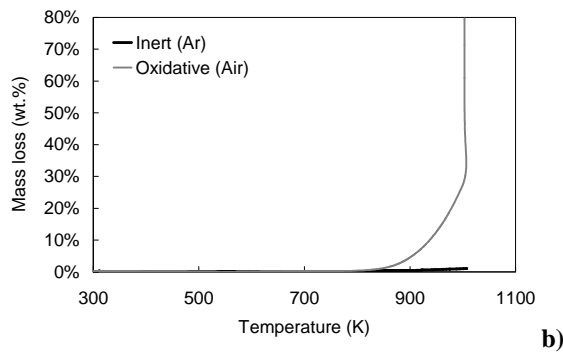
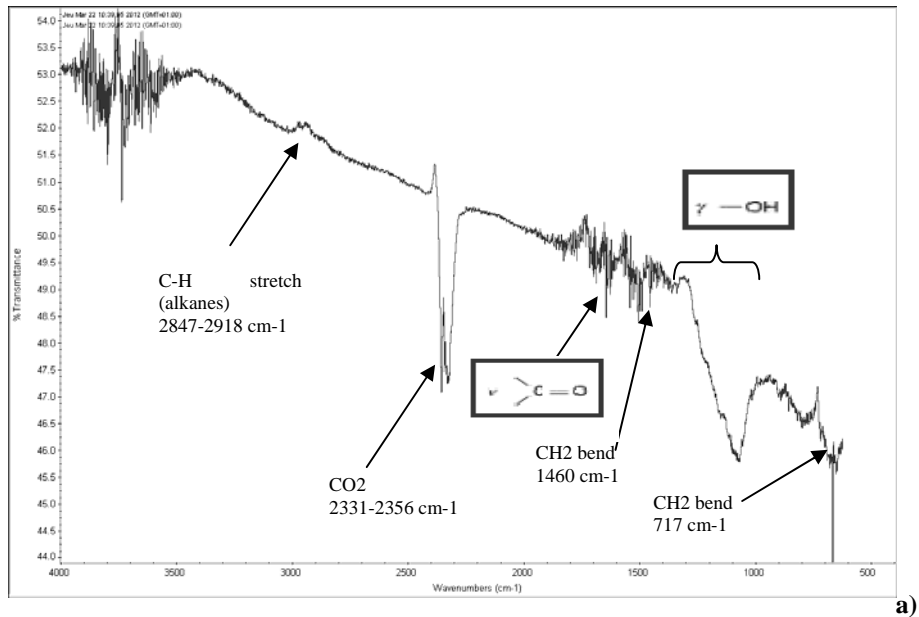
216

217

218

In addition, it can be mentioned that the pressure in the combustor is lower than what could be expected through 0-D calculations with the equilibrium code CEA (considering the following conditions: isentropic case, rocket mode with known specificity of the nozzle, infinite area of the combustion chamber to ensure the completeness of the combustion). Thus, assuming the difference between the experiments and the computation is due to the unburned

219 fuel, it is possible to determine the amount of fuel which did not participate to the combustion. As a consequence, it
 220 is found that 1.7 g.s^{-1} , among the mean value of 5.6 g.s^{-1} , is lost (a flow rate of 3.9 g.s^{-1} is required numerically to
 221 obtain the same pressure as the one measured experimentally). This is about one third of the fuel conversion. This is
 222 a major result since this contributes to explain the low HDPE regression rate. This constitutes a way of research for
 223 future work if one would require enhancing the HDPE regression.



226 **Figure 8. FTIR-DR analysis (a) and Thermogravimetric Analysis of the collected solid particles under inert**
 227 **and oxidative atmosphere (b).**

228 *Analysis of the entire test campaign*

229 The data gathered for the five tests have been post-processed (Table 3). The mean fuel flow rate was estimated
 230 first through the regression rate measures by thermocouples (in conformity with previous section) and second by
 231 weighting the solid reducer before and after the test. A good agreement is obtained (4.2 wt.% of discrepancy). The

232 maximum regression rate is obtained for the higher oxygen content (test number 5870). Furthermore, the solid
 233 reducer is geometrically measured after the test to verify its spatial regression. Nevertheless, the liquefied layer
 234 probably solidifies downstream when the test is stopped, which disables analysing the final geometry of the solid
 235 grain. Considering the solid fuel ejected at the combustor outlet, as explained in the previous section, 10 wt.% to 20
 236 wt.% of the total solid fuel do not react in the combustor (since the theoretical pressure computed with the CEA
 237 code is higher than the experimental one). On the basis of the regression, the equivalence ratio is estimated. It ranges
 238 from 0.53 to 1.06. Most of the tests are thus conducted under lean regime (excess of oxygen). This explains the
 239 ablation of the nozzle, which can be linked to the equivalence ratio. The maximum erosion is found for the
 240 maximum oxygen content (nozzle ablation speed of $90 \mu\text{m.s}^{-1}$). Since the combustion temperature is linked to the
 241 equivalence ratio, the oxygen effect is also a thermal effect. The pressure yield (ratio of the experimental pressure
 242 divided by the theoretical pressure computed for adiabatic combustion) varies from 0.87 to 0.98 which shows the
 243 good combustor efficiency. The thrust and the maximum conduction heat flux computed in the solid fuel thanks to
 244 the thermocouples are also given (Table 3). The conduction heat flux is obtained in cylindrical coordinates using the
 245 temperature measures in the solid fuel grain and their positions. Except for the test number 5866, these two
 246 parameters are linearly linked.

247 **Table 3. Post-processing of test data.**

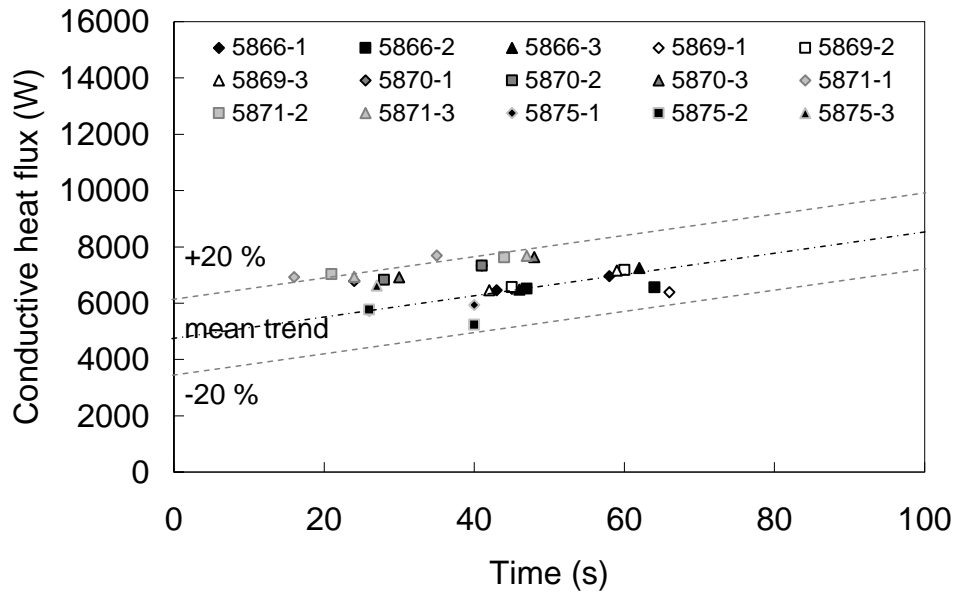
Test number	Mean regression rate			Mean equivalence ratio	Increase of the nozzle diameter (mm)	Pressure yield ()	Thrust (N)	Conduction heat flux (W)
	Measured by thermocouples		Measured by weight loss					
	(mm.s ⁻¹)	(g.s ⁻¹)						
5866	0.2	4.8	5.02	1.06	1.0	0.92	49	7081
5869	0.18	4.3	4.29	0.93	0.1	0.98	79	6555
5870	0.26	6.48	6.58	0.62	4.1	0.87	86	7315
5871	0.18	4.5	4.91	0.53	4.5	0.95	99	7847
5875	0.17	4.19	4.54	0.97	0.1	0.94	62	5505

248

249 Similarly to the results post-processed in **Figure 5**, the regression rate has been estimated thanks to each
 250 thermocouple inserted in the solid fuels (15 per test). The values range from 0.132 mm.s^{-1} to 0.239 mm.s^{-1} without
 251 clear trend. For some tests, the higher value are found at the reducer upstream, for others in the middle or
 252 downstream; this changes during the test duration without understandable effect of one or another parameter on

253 these variations. Consequently, the analysis presented for the test number 5866 in previous section cannot be easily
254 generalized by taking the pressure or the oxidiser effect into account. While in test 5866, the inner diameter of the
255 reducer along the combustor tended to decrease when reaching the outlet, this trend is not found in other test. This
256 point is complex to explain since it is related to the pressure, to the oxidiser content and surface flow rate, to the
257 nozzle throat and to its ablation. One possible explanation on the basis of the observations during the tests is that at
258 the beginning of the test the regression is higher upstream and this impacts the cross-section area which is higher
259 upstream than downstream. The surface mass flow rate of oxidiser is modified and this increases the regression
260 downstream. Finally, at the end of the test, the combustion channel presents a uniform cross-section. This analysis is
261 supported by some thermocouples analysis and by the visualisation of the solid fuel grains of the tests which were
262 stopped before consuming them entirely.

263 The maximum instantaneous conduction heat flux has been estimated for each thermocouple and for each test. A
264 linear relationship (mean trend) is found as a function of the time (**Figure 9**). The values oscillate around this mean
265 line by $\pm 20\%$. This implies that the operating conditions play a role on this heat transfer but it is limited. The fact
266 that the heat flux is not stable from 0 s to 60 s illustrates the fact that due to the solid regression (impacting the
267 equivalence ratio) and to the nozzle damage, a transient evolution of the combustion parameters is found. Regarding
268 the heat flux density for comparison with previous work, the minimum value is measured at $320 \text{ kW}\cdot\text{m}^{-2}$ and the
269 maximum one around $424 \text{ kW}\cdot\text{m}^{-2}$. The previous analytical calculation gave $380 \text{ kW}\cdot\text{m}^{-2}$ [29], which is in good
270 agreement with these measured data.

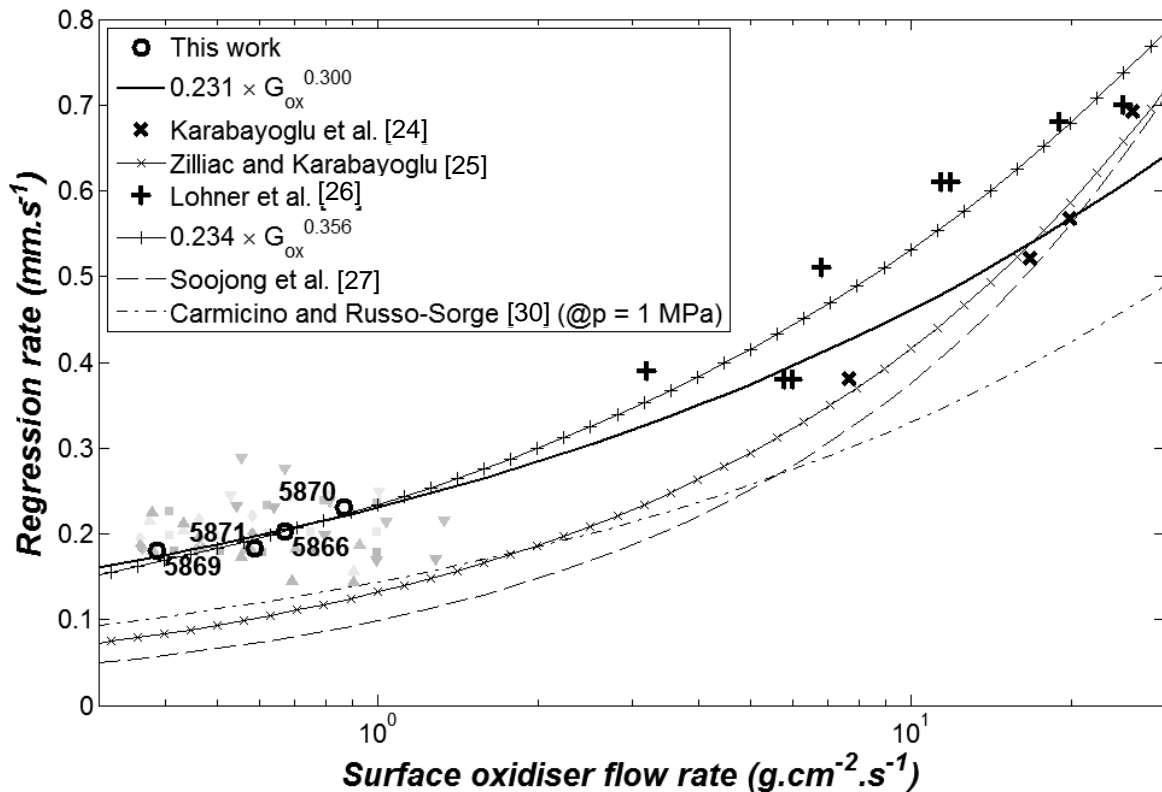


271
 272 **Figure 9. Maximum instantaneous conductive heat flux within the solid reducer as a function of time for all**
 273 **the tests.**

274 Finally, the regression data have been post-processed according to the Marxman law (Eq. 1) [28]. All the data
 275 (one for each thermocouple) are given and the mean values (one per test, marked on **Figure 10** with circle and with
 276 test number) can be fitted by such an exponential law. The parameters found in this work are $a = 0.231$ and
 277 $b = 0.300$. They can be compared with those from Karabayoglu *et al.* [24] ($a = 0.143, b = 0.468$), from Zilliac and
 278 Karabeyoglu [25] ($a = 0.132, b = 0.498$), from Lohner *et al.* [26] ($a = 0.234, b = 0.356$), from Soojong *et al.* [27]
 279 ($a = 0.0988, b = 0.356$) and from Carmicino and Russo-Sorge [30] ($a = 0.144, b = 0.36$). A good agreement is
 280 found, particularly with the work of Lohner *et al.*. This is particularly interesting because the present data are
 281 obtained for an oxidiser flow rate much lower than previous work from the literature. Thus, this enlarges the
 282 applicability of the Marxman law.

$$\dot{r} = a \cdot Q_{ox}^b \quad (1)$$

284 Where \dot{r} is the regression rate, Q_{ox} the oxidizer flow rate, a and b the solid fuel parameters.



285
286
287
Figure 10. Post-processing of the regression rates according to the Marxman law.

288 Conclusion

289 The hybrid rocket engine presents the advantage of a low cost and safe technology. Scientifically, it is required
290 to understand how the heat release rate in the combustor can impact the solid fuel regression to enhance the
291 generation of combustible fuel and the engine's thrust. As a first step in the present work, the hybrid combustor was
292 presented and the results of the five main tests are detailed. Several parameters were varied to estimate their effects.
293 The regression rate was found to vary from $0.132 \text{ mm}\cdot\text{s}^{-1}$ to $0.239 \text{ mm}\cdot\text{s}^{-1}$ on the basis of thermocouple signals. It
294 was correlated to mass loss measurements with a good agreement (less than 10 wt.%). The longitudinal and radial
295 regressions were investigated but the effects of the pressure, of the oxidiser flow rate and of its nature were not
296 clearly quantified because of the difficulty to dissociate these coupled parameters. A stabilisation time has been
297 estimated for the engine around 25 s. The maximum conduction heat flux was determined in the solid fuel and
298 linked to the thrust, which is important to understand the heat and mass transfer coupling in the system. This thrust
299 and the regression rate (due to its relationship with the equivalence ratio) are negatively impacted by the fact that

300 solid particles are formed during the pyrolysis and that they are ejected by the flow without being burned. Thus, a
301 part of the heat flux used to pyrolyse the fuel is lost through the ejection of these combustible particles. This
302 unburned fuel quantity is about one third the one which is pyrolysed during the solid regression. A nozzle throat
303 ablation has been identified due to the oxygen excess (equivalence ratio often lower than 1). Finally, the data were
304 post-processed according to the Marxman law and its parameters are in good agreement with the literature.

305 **References**

- 306 [1] Chiaverini, MJ, Kuo, KK. Fundamentals of Hybrid Rocket Combustion and Propulsion, Progress in
307 Astronautics and Aeronautics, AIAA, Vol. 218, 2007.
- 308 [2] Maggi F, Gariani G, Galfetti L, DeLuca LT. Theoretical analysis of hydrides in solid and hybrid rocket
309 propulsion, Int J Hydrogen Energ 2012; 37(2): 1760-1769.
- 310 [3] Greatrix DR. Regression rate estimation for standard-flow hybrid rocket engines, Aerosp Sci Technol 2009;
311 13(7): 358-363.
- 312 [4] DeLuca LT, Galfetti L, Maggi F, Colombo G, Merotto M, Boiocchi M, Paravan C, Reina A, Tadini P, Fanton
313 L. Characterization of HTPB-based solid fuel formulations: Performance, mechanical properties, and
314 pollution, Acta Astronaut 2012; 10.1016/j.actaastro.2012.05.002.
- 315 [5] Cheung WS, Tilston JR, Testing of a novel propulsion system for micro air vehicles, P I Mech Eng G-J Aer
316 2001; 215(4): 207-218
- 317 [6] Carmicino C and Russo Sorge A. Role of Injection in Hybrid Rockets Regression Rate Behavior, J Propul
318 Power 2005; 21(4)
- 319 [7] Davydenko NA, Gollender RG, Gubertov AM, Mironov VV, Volkov NN. Hybrid rocket engines: The
320 benefits and prospects, Aerosp Sci Technol 2007; 11: 55–60.
- 321 [8] Stone D, Lindenmoyer A, French G, Musk E, Gump D, Kathuria C, Miller C, Sirangelo M, Pickens T.
322 NASA's approach to commercial cargo and crew transportation, Acta Astronaut 2008; 63: 192-197.
- 323 [9] Karabeyoglu MA, Altman D, Cantwell BJ. Combustion of Liquefying Hybrid Propellants: Part 1, General
324 Theory, J Propul Power 2002; 18(3): 610-620.
- 325 [10] Altman D. Rocket Motors, Hybrid, Encyclopedia of Physical Science and Technology (Third Edition), 2004,
326 303-321

- 327 [11] Gariani G, Maggi F, Galfetti L. Numerical simulation of HTPB combustion in a 2D hybrid slab combustor,
328 Acta Astronaut 2011; 69(5–6): 289-296.
- 329 [12] Salva JJ, Tizon JM, Jenaro G, Lopez Agudo C. Numerical analysis of heterogeneous combustion in a ducted
330 rocket, P I Mech Eng G-J Aer 2007; 221(1): 115-127.
- 331 [13] Antoniou A and Akyuzlu KM. A Physics Based Comprehensive Mathematical Model to Predict Motor
332 Performance in Hybrid Rocket Propulsion Systems, in: 41st AIAA/ASME/SAE/ASEE Joint Propulsion
333 Conference & Exhibit 10 - 13 July 2005, Tucson, Arizona, paper n°AIAA 2005-3541
- 334 [14] Karabeyoglu MA and Cantwell BJ. Combustion of Liquefying Hybrid Propellants: Part 2, Stability of Liquid
335 Films, J Propul Power 2002; 18(3): 621-630.
- 336 [15] Karabeyoglu MA, Zilliac G, Cantwell BJ, DeZilwa S, Castellucci P. Scale-Up Tests of High Regression Rate
337 Paraffin-Based Hybrid Rocket Fuels, J Propul Power 2004; 20(6): 1037-1045.
- 338 [16] Cai G, Zeng P, Li X, Tian H, Yu N. Scale effect of fuel regression rate in hybrid rocket motor, Aerosp Sci
339 Technol 2011; 10.1016/j.ast.2011.11.001.
- 340 [17] Nagata H, Ito M, Maeda T, Watanabe M, Uematsu T, Totani T, Kudo I. Development of CAMUI hybrid
341 rocket to create a market for small rocket experiments, Acta Astronaut 2006; 59(1–5): 253-258.
- 342 [18] Zheng G, Wichman IS, Bénard A. Opposed-Flow Flame Spread Over Polymeric Materials: Influence of
343 Phase Change, Combust Flame 2001; 124: 387–408.
- 344 [19] Han CY. Radiative combustion of pyrolyzing fuel in a cylindrical combustor, Fuel 2004; 83: 343–351.
- 345 [20] Cantrell RH, Hart RW, McClure FT. Combustion Instability in Solid Propellant Rockets: Linear Acoustic
346 Gains and Losses in Solid Propellant Rocket Motors, AIAA J 1964; 2(6): 1100-1135.
- 347 [21] Cantrell RH. Gas-Film Effects in the Linear Pyrolysis of Solids, AIAA J 1963; 1(7): 1544-1560.
- 348 [22] Jackson TL and Buckmaster J. Heterogeneous Propellant Combustion, AIAA J 2002; 40(6).
- 349 [23] Chiaverini MJ, Serin N, Johnson DK, Lu YC, Kuo KK, Risha GA. Regression Rate Behavior of Hybrid
350 Rocket Solid Fuels, J Propul Power 2000; 16(1).
- 351 [24] Karabeyoglu MA, Cantwell BJ, Stevens J. Evaluation of Homologous Series of Normal-Alkanes as Hybrid
352 Rocket Fuels, in: 41st AIAA/ASME/SAE/ASEE Joint Propulsion Conference & Exhibit; Tucson, AZ; USA;
353 10-13 July 2005, paper n° AIAA-2005-3908

- 354 [25] Zilliac G and Karabeyoglu MA. Hybrid Rocket Fuel Regression Rate Data and Modeling, in: 42nd
355 AIAA/ASME/SAE/ASEE Joint Propulsion Conference & Exhibit. Sacramento (California), Sacramento,
356 California, July 9-12, 2006, paper n° AIAA-2006-4504.
- 357 [26] Lohner K, Dyer J, Doran E, Dunn Z, Zilliac G. Fuel Regression Rate Characterization Using a Laboratory
358 Scale Nitrous Oxide Hybrid Propulsion System, in: 42nd Joint Propulsion Conference, Sacramento,
359 California, July 9-12, 2006, paper n° AIAA-2006-4671,
- 360 [27] Soojong K, Jungpyo L, Heejang M, Honggye S, Jinkon K, Jungtae C. Effect of Paraffin-LDPE Blended Fuel
361 in Hybrid Rocket Motor, in: 46th AIAA/ASME/SAE/ASEE Joint Propulsion Conference & Exhibit.
362 Nashville, TN, July 25-28, 2010, paper n° AIAA-2010-7031.
- 363 [28] Marxman G and Gilbert M. Turbulent Boundary Layer Combustion in the Hybrid Rocket, 9th International
364 Symposium on Combustion, Academic Press, 1963, 371-372
- 365 [29] Gascoin N, Gillard P, Mangeot A, Navarro-Rodriguez A. Literature survey for a first choice of a fuel-oxidiser
366 couple for hybrid propulsion based on kinetic justifications, J Anal Appl Pyrol 2012; 94: 1-9.
- 367 [30] Carmicino C and Russo Sorge A. Performance comparison between two different injector configurations in a
368 hybrid rocket, Aerosp Sci Technol 2007; 11(1): 61-67.